Robust helical edge transport at $\nu = 0$ quantum Hall state

G. M. Gusev,[1] D. A. Kozlov,[2,3] A. D. Levin,[1] Z. D. Kvon,[2,3] N. N. Mikhailov,[2] and S. A. Dvoretsky[2]
[1]*Instituto de Física da Universidade de São Paulo, 135960-170, São Paulo, SP, Brazil*
[2]*Institute of Semiconductor Physics, Novosibirsk 630090, Russia*
[3]*Novosibirsk State University, Novosibirsk 630090, Russia*
(Received 19 September 2016; published 21 July 2017)

Among the most interesting predictions in two-dimensional materials with a Dirac cone is the existence of the zeroth Landau level (LL), equally filled by electrons and holes with opposite chirality. The gapless edge states with helical spin structure emerge from Zeeman splitting at the LL filling factor $\nu = 0$ gapped quantum Hall (QH) state. We present observations of a giant, nonlocal, four-terminal transport in zero-gap HgTe quantum wells at the $\nu = 0$ QH state. Our experiment clearly demonstrates the existence of the robust helical edge state in a system with single-valley Dirac cone materials.

DOI: 10.1103/PhysRevB.96.045304

Two-dimensional (2D) massless Dirac fermions in the presence of a strong perpendicular magnetic field show several remarkable features that sharply diverge from conventional behavior [1–8]. The energy spectrum is organized in Landau levels (LLs) with square root versus linear dependence on the magnetic field and square root dependence on the Landau index n versus $n + 1/2$, in comparison with the parabolic dispersion at the zero field. The most remarkable consequence of this last property is the existence of a zero-energy LL ($n = 0$). This is not due to the linear spectrum, but is related to the π Berry phase carried by each Dirac point. Therefore, the $n = 0$ LL has a magnetic field independent energy, which is quite different from a quantized cyclotron orbit in the conventional quantum Hall effect (QHE). It is important to find a clear experimental signature that can help to identify zeroth LL in many Dirac materials, such as graphene [2], three-dimensional topological insulators [9], and Weyl semimetals [10].

The existence of the zeroth LL has been examined by measurements of the integer QHE in graphene [2]. Previous experiments in samples with moderate mobility provide indirect evidence of the QHE around filling factor $\nu = 0$: The Hall conductivity has a peculiar plateau at $\sigma_{xy} = 0$ that is not precisely quantized as other plateaus are, and its longitudinal resistivity does not vanish [11]. But this interpretation is based on the bulk spectrum scenario [(Fig. 1(a)]. Note, however, that understanding of the QHE at $\nu = 0$ requires a presence of edge states similar to the conventional integer QHE. In this case, the interpretation becomes ambiguous and depends on the particular structural properties of graphene. In particular, one of the scenarios predicts that, if spin splitting is larger than valley splitting, the bulk LL forms two counterpropagating edge states [12] similar to 2D topological insulators [13] as shown in Fig. 1(b). It is worth noting that unambiguous experimental support for the existence of counterpropagating edge states is provided by nonlocal measurements. The helical edge state transport at $\nu = 0$ differs from the chiral edge mode transport for a higher LL: chiral states carry the same chemical potential in the vicinity of each boundary, while countercirculating edge states carry potential from different current probes (left and right). As a result, conductance is zero in the QHE regime and quantized in universal units $2e^2/h$ in the quantum Hall (QH)-metal regime in the absence of backscattering between spin-polarized states. Several attempts have been made to study nonlocal transport in graphene; however, opposing or conflicting interpretations have been offered [14,15]. Very recently, observation of the quantized local and nonlocal resistances in a single layer [16] and in bilayer [17] graphene of micrometer-sized samples in the presence of a strong in-plane magnetic field have been reported, which has been attributed to the parallel B-induced helical edge modes. Applications of other materials that posses a single Dirac cone is of particular interest.

Recently, a 2D system with a single Dirac cone spectrum, based on HgTe quantum wells, has been discovered [18,19]. The single-spin degenerate Dirac valley allows unambiguous identification of the features resulting from the bulk zeroth LL. In addition, the high mobility and giant Lande g-factor (∼55) favor the formation of spin-polarized counterpropagating states. In this paper, we study the nonlocal transport in ten-probe devices fabricated from HgTe zero-gap quantum structures. We observe a magnetic-field-induced, giant, nonlocal resistance peak near the CNP in different configurations of current and voltage probes. The nonlocal response is comparable with local resistance and increases rapidly with B. The nonlocal resistance persists in magnetic fields up to 7 T. Simple Kirchhof-based estimations and more complicated edge state+bulk model calculations clearly confirm the existence of helical edge states originating from the bulk zeroth LL.

Quantum wells $Cd_{0.65}Hg_{0.35}Te/HgTe/Cd_{0.65}Hg_{0.35}Te$ with (013) surface orientations and a well thickness of 6.3, 6.4, and 6.6 nm were prepared by molecular beam epitaxy. A detailed description of the sample structure has been given in Refs. [19,20]. The sample is a Hall bar device with eight voltage probes. The bar has a width W of 50 μm and three consecutive segments of different lengths L (100,250,100 μm) (Fig. 2). A dielectric layer was deposited (100 nm of SiO_2 and 100 nm of Si_3Ni_4) on the sample surface and then covered by a TiAu gate. The density variation with gate voltage was $1 \times 10^{11} \mathrm{cm}^{-2} V^{-1}$. The magnetotransport measurements were performed in the temperature range $1.4 - 70K$ using a standard four-point circuit with a $1 - 13Hz$ ac current of $1 - 10nA$ through the sample, which is sufficiently low to avoid overheating effects. It is worth noting that the electrical contacts to the electron gas beneath the gate electrode become worse in a strong magnetic field, therefore we report the results

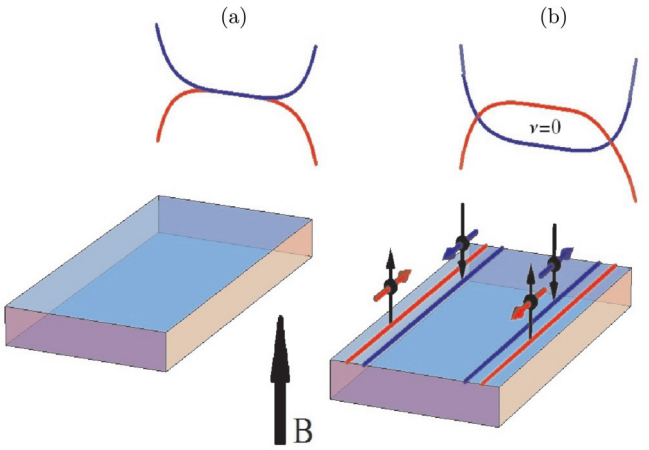

FIG. 1. Schematics of band structure (energy spectrum) in (a) low and (b) high magnetic field, showing the zero LL in the middle of the sample and at the sample edge, and counterpropagating spin-polarized edge states in a slab-shaped sample for the $\nu = 0$ LL state.

up to 5 or 7 T (depending on the particular device). Ten devices from three different wafers were measured, all with similar results.

Figure 2 shows the zero field, longitudinal R_{xx}, Hall R_{xy}, and nonlocal R_{NL} resistances measured in a perpendicular magnetic field B=5 T as a function of gate voltage. R_{xx} and R_{xy} are measured in multiterminal Hall bar geometry. In the local configuration, the current flows between contacts 1,6; voltage is measured between probes 3,4 ($R_L = R_{xx} = R_{1-6,3-4} = V_{3,4}/I_{1,6}$); and Hall voltage is measured between probes 3,9 ($R_{xy} = R^{3,9}_{1,6} = V_{3,9}/I_{1,6}$). In the nonlocal configuration, the current flows between contacts 2,10 and voltage is measured between probes 3,9 ($R_{NL} = R^{3,9}_{2,10} = V_{3,9}/I_{2,10}$). Zero-field resistance behavior resembles behavior in other HgTe-based quantum wells, including topological insulators [13,19–22] and semimetals [23,24]: resistance shows a peak around the charge neutrality point (CNP). In graphene and zero-gap HgTe wells, the CNP is coincident with the Dirac point [5,7,18,19]. The maximum resistivity at the Dirac point $\rho_{xx} = \frac{W}{L} R^{3,4}_{1,6}(0) = 0.3\frac{h}{e^2}$ agrees with others' observations [18,20].

When we applied an external perpendicular magnetic field, a pronounced anomaly in the resistance data was observed: resistance was found to increase very strongly with B near the CNP, while in other regions the system demonstrates conventional QH behavior (Fig. 2). Evolution of the local $R_L = R^{3,4}_{1,6} = V_{3,4}/I_{1,6}$ and nonlocal $R_{NL} = R^{3,9}_{2,10} = V_{3,9}/I_{2,10}$ resistances with gate voltage and magnetic field is shown in Fig. 3. Both R_L and R_{NL} exhibit sharp peaks above the critical magnetic field $B_c \sim 2.5T$. Nonlocality is absent in the magnetic field below B_c.

The important difference between the QH states with $\nu = 0$ and $\nu \neq 0$ is that, in the conventional quantization regime, the longitudinal transport coefficient vanishes in both conductivity σ_{xx} and resistivity ρ_{xx}, while for the QHE state in $\nu = 0$ this is not necessarily the case $\rho_{xx} = 0$. Indeed, we obtain $\sigma_{xy} \sim \sigma_{xx} \sim 0$ because $\rho_{xx} \gg \rho_{xy}$ at $\nu = 0$ [25]. Note that for the Hall insulating state it is expected that both longitudinal and Hall resistivities are going to infinity near the

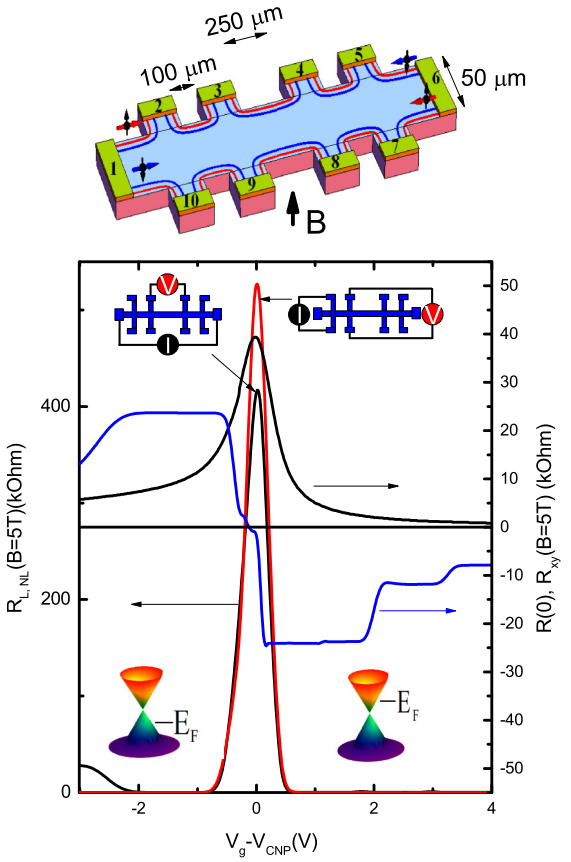

FIG. 2. Top—a schematic of device (not preserving aspect ratio) and the local zero-field resistance R(0), longitudinal $R_L = R_{xx}$ (I=1,6, V=3,4)(black curve) Hall R_{xy} (I=1,6; V=3,9)(blue curve) and nonlocal R_{NL} (I=2,10; V=3,9) (red curve) resistances as a function of gate voltage at B=5 T, T=4.2 K, I = 10^{-9}A. The schematics show how the current source and the voltmeter are connected for the measurements.

CNP in accordance with the classical Hall resistivity formula $\rho_{xy} \sim B/(n-p)ec$, where n and p are electron and hole densities, respectively, if we assume the same mobility for both carrier types. Divergent longitudinal and vanishing Hall resistivities have been observed at the Dirac point in graphene and attributed to density inhomogeneities associated with electron-hole puddles [26]. The alternative approach to the $\nu = 0$ QHE was based on counterpropagating edge channels with opposite spin directions [12]. In this model, the Hall resistance is zero because of compensation between the helical states in accordance with Landauer-Buttiker formalism, while the resistance measured between probes is quantized in units of $h/2e^2$ in the ballistic case and much higher than the resistance quantum in the diffusive case, similar to a 2D topological insulator in zero magnetic field [22,27].

We provide evidence that advances this debate by measuring the long-range nonlocal transport in the QHE regime in Dirac cone materials. For example, because graphene has two valleys, two different situations must be considered, depending on whether the bulk valley splitting is larger or smaller than the bulk spin splitting in the zeroth LL. If the valley degeneracy lifts first, and valley separation becomes larger than

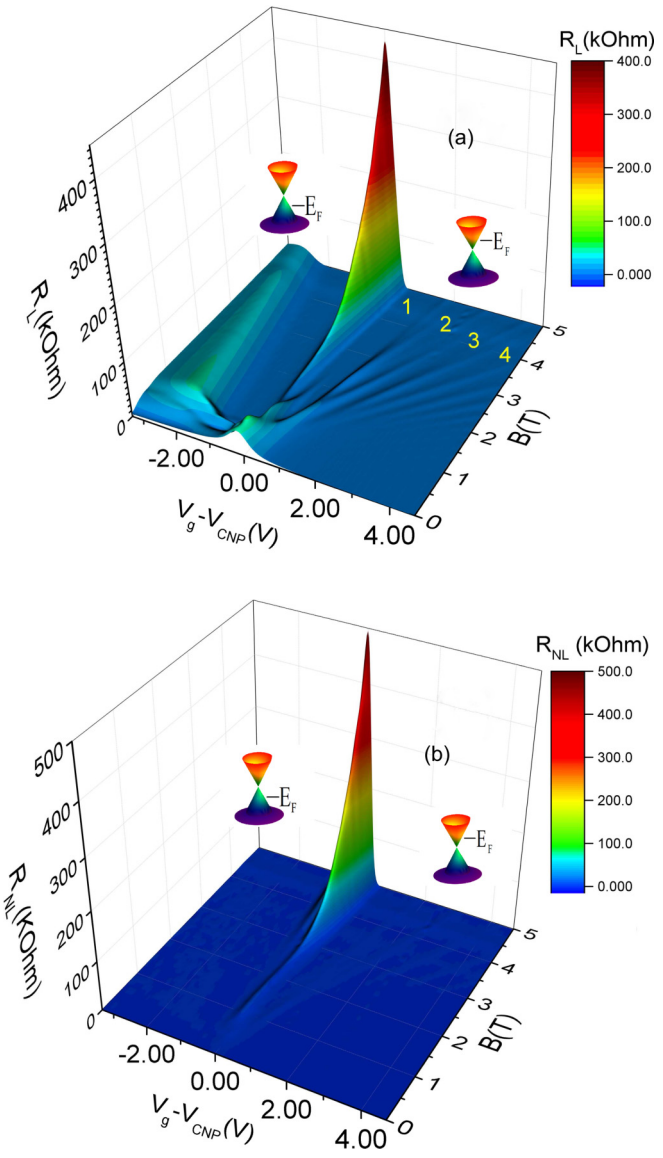

FIG. 3. (a) The local $R_L = R_{xx}$ (I=1,6, V=3,4) and (b) nonlocal R_{NL} (I=2,10; V=3,9) resistances as a function of the gate voltage and magnetic field, T=4.2K. Filling factors determined from Hall resistance are labeled.

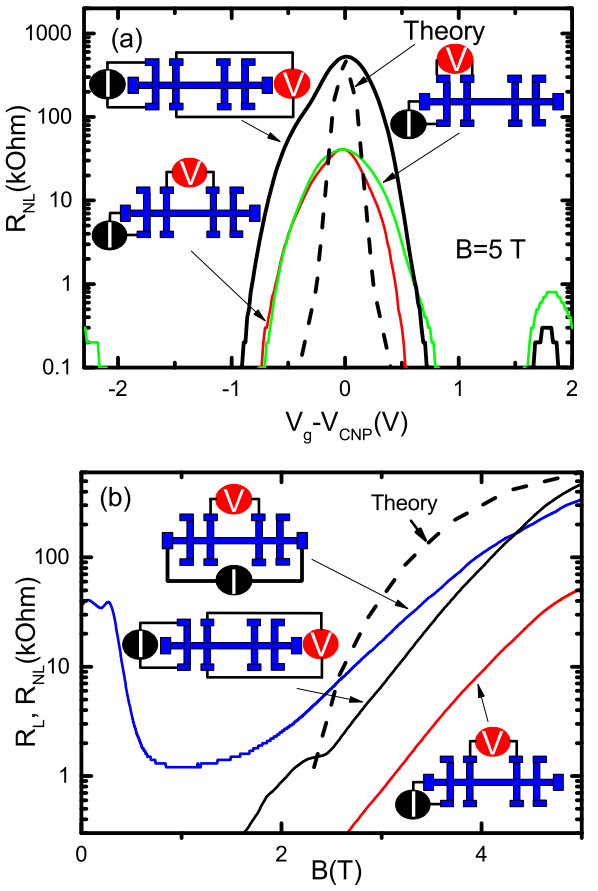

FIG. 4. (a) The nonlocal R_{NL} resistances as a function of gate voltage at B=5 T, T=4.2 K, obtained for different measuring configurations. Dashes—nonlocal resistance R_{NL} (I=2,10; V=3,9) calculated from model [25]. (b) Comparison of the magnetic field dependencies for both local and nonlocal resistances in various configurations obtained at the CNP. Dashes—nonlocal resistance R_{NL} (I=2,10; V=3,9) calculated from model [25]. The schematics show how the current source and the voltmeter are connected for the measurements.

the Zeeman energy, the edge states do not cross and the gap appears both in the bulk and at the edges of the sample. Such a QH insulator resembles common insulators without edge states. The other possibility occurs when the Zeeman energy is larger than the valley splitting. The electronlike (holelike) LL bends upwards (downwards) in energy near the edge of the sample and forms two counterpropagating edge states residing on the same edge [Fig. 1(b)]. Such QH metal resembles a nontrivial topological insulator in a zero magnetic field with a bulk gap and helical edge states protected by the time reversal symmetry against backscattering [13]. The mechanism of the lift of fourfold degeneracy and the existence of a possible insulating state in graphene have been discussed extensively [28–32]. A high-field insulating state has been observed in both low- and high-quality graphene samples. The general consensus is that the magnetic field drives graphene at the CNP from the QH-metal state at a relative low field into the QH-insulator state at a high-enough field.

Figure 4(a) illustrates R_{NL} for various configurations measured at a fixed magnetic field B=5T. Figure 4(b) shows the magnetic field dependence of both local and nonlocal resistances at a fixed gate voltage corresponding to the CNP. One can see almost exponential growth of R_L and R_{NL} above B_c. In the magnetic field region $0.3T < B < 1.4T$, the experimental local resistance shows complex and diverse behavior: it reveals a large negative magnetoresistance and plateauxlike features. Previously [20], these features have been attributed to the emergence of the zeroth LL without edge states (Fig. 1(a)], which is represented by a sharp peak near the CNP in $\sigma_{xx}(V_g)$. When the magnetic field is such that the bulk Zeeman gap is larger than the zeroth LL broadening Γ, which occurs at $B_c \approx \Gamma/g\mu_B \approx 2.5T$, where μ_B is the Bohr magneton, one expects nonlocal transport due to the helical edge states. The nonlocal resistance is strongly suppressed at high temperatures, while the local resistance is found to be much more robust [25].

To get more insight into the physics of the observed nonlocality, it is important to estimate the phenomenon theoretically. To explain the value of the local and nonlocal resistances in most of the experimental observations mentioned above, a simple picture of the helical edge state is usually enough. We have seen that, using Kirchhoff's laws, we can analyze our circuit. There is a simple expression that allows one to calculate the resistance value for any measurement configuration assuming that there is only edge state transport in the sample [27]: $R^{i,j}_{n,m} = \frac{L_{n,m}L_{i,j}}{Ll}(h/e^2)$, where $R^{i,j}_{n,m}$ is the voltage measured between contacts i and j while the current is maintained between contacts n and m, $L_{i,j}$ ($L_{n,m}$) are the distances between i and j (n and m) along the gated sample edge that does not include n and m (i and j), L is the total perimeter of the sample, and l is the mean free path due to the scattering between helical states propagated along the same edge. Assuming a homogeneous material and that the mean path remains constant along the edge, we obtain the ratio between nonlocal and local resistances: $R_{NL}/R_L = R^{3,9}_{2,10}/R^{3,4}_{1,6} = 2$; $R_{NL}/R_L = R^{2,3}_{1,10}/R^{3,4}_{1,6} = 0.11$; $R_{NL}/R_L = R^{3,4}_{1,10}/R^{3,4}_{1,6} = 0.125$. The result of these calculations is close to the experimental result: $(R_{NL}/R_L)^{\rm exp} = R^{3,9}_{2,10}/R^{3,4}_{1,6} = 1.1-1.75$; $(R_{NL}/R_L)^{\rm exp} = R^{2,3}_{1,10}/R^{3,4}_{1,6} = 0.08-0.1$; $(R_{NL}/R_L)^{\rm exp} = R^{3,4}_{1,10}/R^{3,4}_{1,6} = 0.07-0.1$. There is an interesting fact that, in certain sample probe configurations, one can obtain a nonlocal resistance greater than the local one (Figs. 2 and 3).

However, away from the CNP, the current penetrates into the interior of the sample, and the system behaves more and more like a conventional 2D gas. We apply formalism developed in Ref. [10] to describe the local resistance in graphene near $\nu = 0$ in QH metal and then extended it to nonlocal resistance in semimetals [33]. The model explains the transport coefficients in the regime, where the edge-state current is suppressed by bulk contribution to conductivity. The scattering between the edge states and the scattering between bulk states and each of the edge states is characterized by the mean free path $\gamma^{-1} = l$ and g^{-1}, respectively, which are assumed to be smaller than the sample's dimensions [25].

Figures 4(a) and 4(b) display the results obtained from this model for typical parameter values $\gamma^{-1} = 0.33\,\mu$m and $g^{-1} = 0.33\,\mu$m. Clearly, the model reproduces qualitatively the main features of the measurements; in particular, suppression of the peak away from the CNP by bulk contribution to the transport and rapid growth with the magnetic field due to Zeeman splitting. Note that the calculated peak profile is sharper than the measured one. A detailed comparison with the experiment requires knowledge of the density of the states in the gap between the LLs, and ratio between localized and delocalized electrons on the tails of the Gaussian density of states in the QH regime.

A number of theoretical models have addressed the evolution of the helical edge states in a magnetic field [34–36]. The results appear to be controversial: While primary models predict that the counterpropagating edge states persist up to a critical magnetic field [34,35], more recent calculations demonstrate the emergence of a gap in the spectrum of the edge states at an arbitrary small B [36]. Such high sensitivity of the edge-state spectrum to the external magnetic field has been attributed to the natural interface inversion asymmetry in HgTe quantum wells. In sharp contrast with this prediction, we observe a giant nonlocal magnetoresistance, which confirms the persistence of the helical states up to 7 T. Note that the effective Hamiltonian which ascribes the bulk energy spectrum and the structure of the edge states in the presence of the perpendicular magnetic field is not properly derived from microscopic theory. For example, another 6×6 matrix Hamiltonian has been successfully applied to the calculation of the energy spectrum in HgTe quantum wells in the presence of an in-plane magnetic field [37]. Further theoretical study is required.

In conclusion, we have studied the local and nonlocal transport properties of the zero LL in a Dirac cone 2D system based on a zero-gap HgTe quantum well. A giant, nonlocal resistance has been observed at the $\nu = 0$ QHE. In comparison with graphene, which is the most typical 2D material with Dirac cones, our system has several advantages. First, the single cone spectrum allows unambiguous interpretation of the integer Hall effect based on the existence of counterpropagating edge states with opposite spin emerging from the zero bulk LL, ruling out the valley first split model in graphene. Secondly, the advantage in fabrication (MBE growth versus exfoliation) allows the production of samples with a large distance between probes and, therefore, justifies the long-range nature of the nonlocal transport due to the edge states.

The financial support of this work by the Russian Science Foundation (Grant No. 16-12-10041, MBE growth of HgTe QWs, fabrication of the field effect transistors and carrying out of the experiment and data analysis), FAPESP (Brazil), and CNPq (Brazil) is acknowledged. The authors thank O. E. Raichev for helpful discussions.

[1] K. S. Novoselov, A. K. Geim, S. V. Morozov, D. Jiang, Y. Zhang, S. V. Dubonos, I. V. Grigorieva, and A. A. Firsov, Science **306**, 666 (2004).

[2] K. S. Novoselov, A. K. Geim, S. V. Morozov, D. Jiang, M. I. Katsnelson, I. V. Grigorieva, S. V. Dubonos, and A. A. Firsov, Nature **438**, 197 (2005); Y. Zhang, Y.-W. Tan, H. L. Stormer, and P. Kim, *ibid.* **438**, 201 (2005).

[3] K. S. Novoselov, E. McCann, S. V. Morozov, V. I. Fal'ko, M. I. Katsnelson, U. Zeitler, D. Jiang, F. Schedin, and A. K. Geim, Nat. Phys. **2**, 177 (2006).

[4] K. S. Novoselov, Z. Jiang, Y. Zhang, S. V. Morozov, H. L. Stormer, U. Zeitler, J. C. Maan, G. S. Boebinger, P. Kim, and A. K. Geim, Science **315**, 1379 (2007).

[5] A. H. Castro Neto, F. Guinea, N. M. R. Peres, K. S. Novoselov, and A. K. Geim, Rev. Mod. Phys. **81**, 109 (2009).

[6] M. Mucha-Kruczynski, E. McCann, and V. I. Falko, Semicond. Sci. Technol. **25**, 033001 (2010).

[7] Xiao-Liang Qi and Shou-Cheng Zhang, Rev. Mod. Phys. **83**, 1057 (2011).

[8] A. A. Burkov and L. Balents, Phys. Rev. Lett. **107**, 127205 (2011).
[9] S. Das Sarma, S. Adam, E. H. Hwang, and E. Rossi, Rev. Mod. Phys. **83**, 407 (2011).
[10] A. K. Geim and A. H. MacDonald, Phys. Today **60**(8), 35 (2007).
[11] J. G. Checkelsky, Lu Li, and N. P. Ong, Phys. Rev. Lett. **100**, 206801 (2008).
[12] D. A. Abanin, K. S. Novoselov, U. Zeitler, P. A. Lee, A. K. Geim, and L. S. Levitov, Phys. Rev. Lett. **98**, 196806 (2007).
[13] M. Konig, S. Wiedmann, C. Brune, A. Roth, H. Buhmann, L. W. Molenkamp, X.-L. Qi, and S.-C. Zhang, Science **318**, 766 (2007).
[14] D. A. Abanin, S. V. Morozov, L. A. Ponomarenko, R. V. Gorbachev, A. S. Mayorov, M. I. Katsnelson, K. Watanabe, T. Taniguchi, K. S. Novoselov, L. S. Levitov, and A. K. Geim, Science **332**, 328 (2011).
[15] J. Renard, M. Studer, and J. A. Folk, Phys. Rev. Lett. **112**, 116601 (2014).
[16] A. F. Young, J. D. Sanchez-Yamagishi, B. Hunt, S. H. Choi, K. Watanabe, T. Taniguchi, R. C. Ashoori, and P. Jarillo-Herrero, Nature **505**, 528 (2014).
[17] P. Maher, C. R. Dean, A. F. Young, T. Taniguchi, K. Watanabe, K. L. Shepard, J. Hone, and P. Kim, Nat. Phys. **9**, 154 (2013).
[18] B. Büttner, C. X. Liu, G. Tkachov, E. G. Novik, C. Brne, H. Buhmann, E. M. Hankiewicz, P. Recher, B. Trauzettel, S. C. Zhang, and L. W. Molenkamp, Nat. Phys. **7**, 418 (2011).
[19] D. A. Kozlov, Z. D. Kvon, N. N. Mikhailov, and S. A. Dvoretskii, JETP Lett. **96**, 730 (2012).
[20] D. A. Kozlov, Z. D. Kvon, N. N. Mikhailov, and S. A. Dvoretskii, JETP Lett. **100**, 724 (2014).
[21] H. Buhmann, J. Appl. Phys. **109**, 102409 (2011).
[22] G. M. Gusev, Z. D. Kvon, O. A. Shegai, N. N. Mikhailov, S. A. Dvoretsky, and J. C. Portal, Phys. Rev. B **84**, 121302(R) (2011).
[23] Z. D. Kvon, E. B. Olshanetsky, D. A. Kozlov *et al.*, Pis'ma Zh. Eksp. Teor. Fiz. **87**, 588 (2008) [JETP Lett. **87**, 502 (2008)].
[24] E. B. Olshanetsky, Z. D. Kvon, N. N. Mikhailov, E. G. Novik, I. O. Parm, and S. A. Dvoretsky, Solid State Commun. **152**, 265 (2012).
[25] See Supplemental Material http://link.aps.org/supplemental/10.1103/PhysRevB.96.045304, which includes Ref. [10], for details on the conductivities measurements and the model that take into account the edge and bulk contribution to the total current in Dirac metal at $\nu = 0$ LL.
[26] S. Das Sarma and Kun Yang, Solid State Commun. **149**, 1502 (2009).
[27] E. B. Olshanetsky, Z. D. Kvon, G. M. Gusev, A. D. Levin, O. E. Raichev, N. N. Mikhailov, and S. A. Dvoretsky, Phys. Rev. Lett. **114**, 126802 (2015).
[28] Y. Barlas, Kun Yang, and A. H. MacDonald, Nanotech. **23**, 052001 (2012).
[29] J. N. Fuchs and P. Lederer, Phys. Rev. Lett. **98**, 016803 (2007).
[30] K. Nomura, S. Ryu, and D. H. Lee, Phys. Rev. Lett. **103**, 216801 (2009).
[31] C. Y. Hou, C. Chamon, and C. Mudry, Phys. Rev. B **81**, 075427 (2010).
[32] I. A. Lukyanchuk and A. M. Bratkovsky, Phys. Rev. Lett. **100**, 176404 (2008).
[33] G. M. Gusev, E. B. Olshanetsky, Z. D. Kvon, A. D. Levin, N. N. Mikhailov, and S. A. Dvoretsky, Phys. Rev. Lett **108**, 226804 (2012).
[34] B. Scharf, A. Matos-Abiague, and J. Fabian, Phys. Rev. B **86**, 075418 (2012).
[35] J.-C. Chen, J. Wang, and Q.-F. Sun, Phys. Rev. B **85**, 125401 (2012).
[36] M. V. Durnev and S. A. Tarasenko, Phys. Rev. B **93**, 075434 (2016).
[37] O. E. Raichev, Phys. Rev. B **85**, 045310 (2012).